Journal of Food Engineering 264 (2020) 109675

Contents lists available at ScienceDirect

Journal of Food Engineering

journal homepage: www.elsevier.com/locate/jfoodeng

Flow process and heating conditions modulate the characteristics of whey protein aggregates.

Domitille de Guibert[a], Marie Hennetier[b], François Martin[a], Thierry Six[c], Yingying Gu[c], Cécile Le Floch-Fouéré[a], Guillaume Delaplace[c], Romain Jeantet[a,*]

[a] STLO, INRA, AGROCAMPUS OUEST, 35042, Rennes, France
[b] EI Purpan, Agro-physiology Laboratory, 31000, Toulouse, France
[c] Unité Matériaux et Transformations (UMET) - UMR 8207, INRA, PIHM Team, 369 rue Jules Guesde, 59651, Villeneuve d'Ascq, France

ARTICLE INFO

Keywords:
Fractal aggregates
Continuous processing
Flow regime
Whey protein
Asymmetrical flow field-flow fractionation

ABSTRACT

Whey protein fractal aggregates reveal different texturizing properties depending on their size. This study characterize the effect of three process parameters (flow regime, heating residence time (RT_h) and heating temperature) on the size and shape of aggregates formed at a semi-industrial scale using a dynamic tubular heat exchanger, and identify the mechanisms involved in their formation. The study showed that physicochemical parameters are not the unique levers to modulate agregates properties but process parameters are also efficient. Asymetrical-Flow-Field-Flow-Fractionation was used to highlight the significant increase of aggregate size produced under transient regime conditions compared to laminar and turbulent regimes. Even larger aggregates were obtained while increasing the heating temperature from 80 to 85 °C since the unfolding aggregation of protein was controlled by the aggregation step. Moreover, RT_h showed no effect on aggregate formation. This study paves the way to the control of aggregate properties obtained in a continuous dynamic mode.

1. Introduction

Whey protein (WP) has been extensively studied with regard to its use in food products. Interest was expressed in the design of WP aggregates (compact sphere, fibril or strand-like) (Jung et al., 2008) at the laboratory scale by adjusting physicochemical conditions in order to obtain new functional properties.

Among WP aggregates, fractal aggregates are soluble aggregates obtained from pure β-lactoglobulin (Blg) (Bon et al., 1999; Nicolai et al., 2011; Pouzot et al., 2005) or from WP solutions (Mahmoudi et al., 2007; Nicolai et al., 2011) at pH 7. A two-step nucleation-growth of this aggregate mechanism has been proposed for static conditions by Nicolai et al. (2011) (Fig. 1.). In a first step, primary aggregates are obtained from the association of denatured monomers, and small oligomers form under heating. Indeed, under heating, protein structure is modified, exposing reactive groups (hydrophobic and thiol groups) at the protein surface and creating bonds through the monomers. A second aggregation favored under high protein concentration then takes place, leading to the association of primary aggregates into larger fractal aggregates. Another way to promote this step is to screen electrostatic charges between primary aggregates by adding salt and/or reducing them by decreasing pH. Large aggregates are formed by nonspecific interactions, not involving –SH groups (Wijayanti et al., 2014).

Fractal aggregates reveal exceptional functional properties depending on their size, such as gel strengtening, thickening properties and the stabilization of emulsions (Chevallier et al., 2016; Kharlamova et al., 2018a; Loiseleux, 2018; Nicolai et al., 2011). For example, Kharlamova et al. (2018a, 2018b) showed that small fractal aggregates (hydrodynamic radius Rh $<$ 35 nm) gelify slower and are less sensitive to syneresis than larger aggregates (Rh $>$ 77 nm); in contrast, large aggregates exhibit better thickening properties (Inthavong et al., 2016). Controlling aggregate size is therefore so a key point to control their functional properties when used in food products.

To date, large fractal aggregate formation has been mainly proposed at the static laboratory scale by indirect heating in a water bath by using high concentrations of protein and salt. For example, Kharlamova et al. (2018a) obtained fractal aggregates with Rh $>$ 500 nm after static heat treatment of a protein solution of 93 $g.L^{-1}$, and Loiseleux et al. (2018) obtained using a static heat treatment fractal aggregates with a gyration radius (Rg) of 209 nm using an initial protein solution at 50 $g.L^{-1}$ with 45 mM NaCl. It is easy to control aggregate size at laboratory scale, but Erabit et al. (2014), working with microgel aggregates, already showed that the control of aggregate size with physicochemical parameters was more difficult under dynamic conditions

* Corresponding author.
E-mail address: romain.jeantet@agrocampus-ouest.fr (R. Jeantet).

https://doi.org/10.1016/j.jfoodeng.2019.07.022
Received 27 March 2019; Received in revised form 18 July 2019; Accepted 24 July 2019
Available online 26 July 2019
0260-8774/

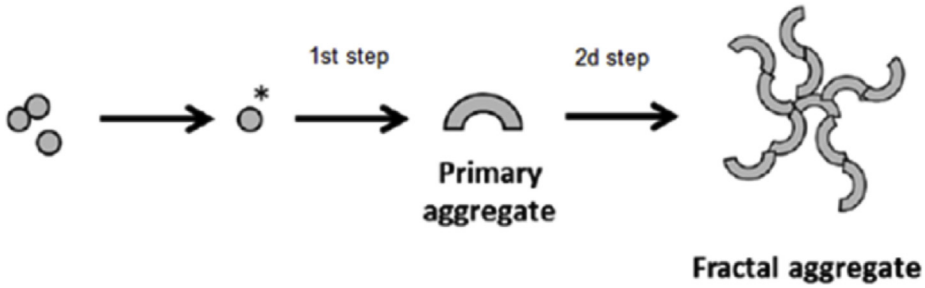

Fig. 1. Scheme of the fractal aggregate formation mechanism. From Chevallier, M. (2017), adapted from Nicolai et al. (2011).

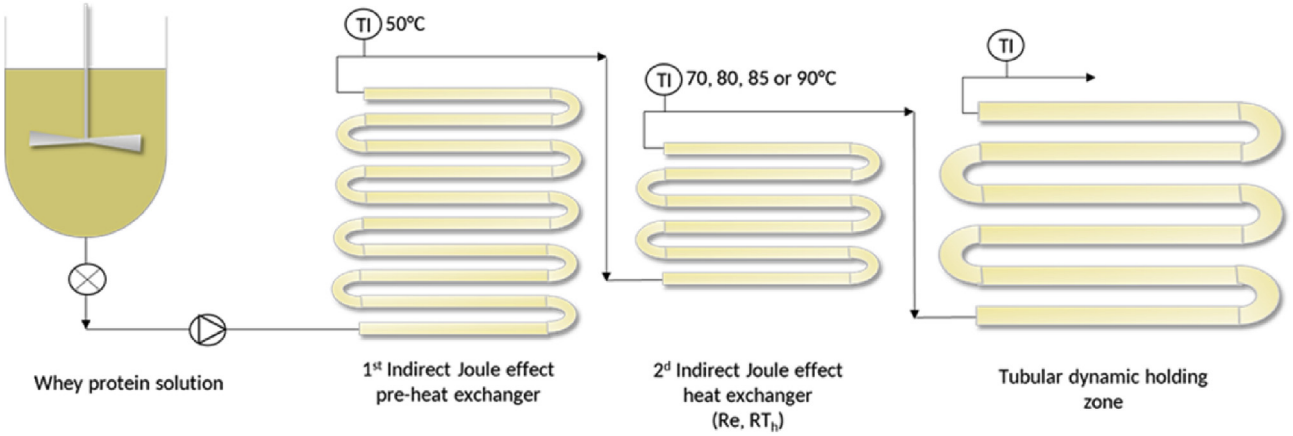

Fig. 2. Schematic representation of the heat treatment pilot.

because of the contribution of shear forces. Several authors have studied the impact of temperature, shear or flow regime on whey protein aggregate size (Erabit et al., 2016; Kerche et al., 2016; Mahmoudi et al., 2014; Simmons et al., 2007; Wolz et al., 2016) but only few authors have produced fractal aggregates at the pilote scale under continuous conditions involving variations of flow regimes and heating residence times (Buggy et al., 2018; Mahmoudi et al., 2014; Nicorescu et al., 2009).

Moreover, in any case, the results of these published studies remain partial and sometimes controversial, especially concerning the influence of shear and flow regime on aggregate size and shape.

The aim of this study was therefore to investigate the influence of process parameters, namely flow regime (assessed by the Reynolds number Re) and residence time (RT_h) in the heating zone, as well as outlet heating temperature, on fractal aggregate formation under continuous conditions in order to control their size. For this reason, a continuous process line was set up at the pilot scale. It consisted of heat-treating a WP solution designed with regard to protein, salt concentration and pH in an indirect Joule effect tubular heat exchanger. Aggregates were then characterized in terms of size, shape and structure by Asymmetrical Flow Field-Flow Fractionation (A4F), which is a suitable method for polydisperse and non-spherical aggregates since it provides higher resolution than SEC for WP components of high molar mass and that can occur at lower concentrations (Kang et al., 2011). Based on this knowledge, the supposed mechanisms involved in the formation of such aggregates under continuous flow conditions were then proposed.

2. Materials and methods

2.1. Protein solution

Whey protein isolate was purchased from a dairy company (confidential information). The powder was composed of 86.5 w/w % of protein that included 7.3 w/w % of casein as determined by SDS-PAGE quantification under reducing conditions. Whey Protein Isolate (WPI) powder was recombined in deionized water at 20 °C under mechanical stirring overnight to reach a concentration of 47 $g.L^{-1}$. Sodium chloride was added to obtain the desired ionic strength of 10 mM, and pH was adjusted to 7.0 by the addition of sodium hydroxyde. These physico-chemical conditions (protein and salt concentrations) were chosen to be the closest to the ideal conditions described in the literature (Chevallier et al., 2016; Kharlamova et al., 2018a; Loiseleux, 2018; Nicolai et al., 2011) but were also adapted to the constraints of the pilot scale.

2.2. Continuous heat treatment

The heat treatment pilot included a feed tank, a first indirect Joule effect Actijoule heat exchanger(Actini, France) (stainless steel: 316L; thermal conductivity: 16.30$W.m^{-1}.K^{-1}$; tube thickness: 10^{-3} m; electrical characteristics: U = 380V; P = 19 kW; I = 28,9A) to pre-heat quickly the protein solution up to 50 °C, a second indirect Joule effect Actijoule tubular heat exchanger (Actini, France) (stainless steel: 316L thermal conductivity: 16.30$W.m^{-1}.K^{-1}$; tube thickness: 10^{-3} m; electrical characteristics: U = 380V; P = 30 kW; I = 45,6A) to control flow conditions and achieve the target outlet heating temperature (70 °C, 80 °C, 85 °C or 90 °C) and a tubular dynamic holding zone to maintain the product at outlet temperature during 15 min (Mean holding time) (Fig. 2).

First, the processing line was equilibrated on water in order to reach the target temperatures. Temperature regulation was done at the end of preheating zone and at the end of heating zone of the heat exchanger using a thermocouple on exchanger outlet wall. A three-way valve then made it possible to switch on the WP solution. The arrival of the product at the outlet of the tube was determined by conductimetry, and the solution was then run for at least 10 min before samples were collected. The experiments were conducted on a complete experimental plan (see supplementary table) over a range from Re 2000 to 25000. The

Table 1
Processing conditions applied to test the influence of residence time (RT_h) and Reynolds number (Re) in the heating section.

	Processing conditions				
	1	2	3	4	5
Flow rate ($L.h^{-1}$)	473	142	379	127	60
Heat exchanger 1					
Inner diameter (m)	0.018	0.018	0.006	0.018	0.018
Number of tubes	12	12	6	12	12
Total length (m)	19.03	19.03	9.1	19.03	19.03
Pre heating temperature (°C)	50	50	50	50	50
Heat exchanger 2					
Inner diameter (m)	0.0225	0.0025	0.018	0.006	0.006
Number of tubes	12	12	12	6	6
Total length (m)	22.82	22.82	19.03	9.1	9.1
Heating Residence Time RT_h (s)	**69**	**230**	**46**	**7**	**15**
Reynolds value Re	**6900**	**2000**	**6900**	**6900**	**3200**

complete plan was used for the statistical analysis. Trials presented in the paper (Table 1) are representative of this complete experimental plan with regard to flow regime and RTh influence, and were repeated in duplicate.

2.3. Moody diagram

The hydraulic performances of the heating section was previously identified by experimental flow tests with a range of sucrose solutions (from 42 w/w % to 66 w/w %) circulating at varying flow rates from 50 to 500 $L\,h^{-1}$ and measuring pressure drop. From these measurements, the Moody diagram was plotted, representing the friction factor evolution as a function of Reynolds number. Analysis of Moody diagram, allowed us to estimate the transition from laminar to turbulent flow by estimating the change in slope. Reynolds number was calculated as:

$$Re = \frac{D\cdot\rho\cdot v}{\mu} \tag{1}$$

Where D is the inner diameter of the pipe (m), ρ is the density of the fluid ($kg.m^{-3}$), v is the flow velocity ($m.s^{-1}$) and μ is the dynamic viscosity (Pa.s). The friction factor f in the tube is given by the Darcy equation:

$$f = \frac{D}{2\cdot\rho\cdot v^2\cdot L}\cdot\Delta P \tag{2}$$

where L is the length of the tube (m) and ΔP is the pressure drop (bar).

2.4. Determining the Kolmogorov length

In order to compare the flow eddy scale to the aggregate size, the Kolmogorov length was determined in turbulent regime using the following equation:

$$l_k = \left(\frac{(\mu/\rho)^3}{E_D}\right)^{1/4} \tag{3}$$

Where l_k is the Kolmogorov length (m), μ/ρ is the cinematic viscosity ($m^2.s^{-1}$) and E_D is the power dissipated per unit mass of fluid ($W.kg^{-1}$), which was calculated as:

$$E_D = \frac{Q\cdot\Delta P}{\rho\cdot V} \tag{4}$$

where Q is the volumetric flow rate ($m^3.s^{-1}$) and $\rho\cdot V$ is the mass of fluid (kg). ΔP was estimated here using Darcy's equation:

$$\Delta P = \frac{Da\cdot v^2\cdot\rho\cdot L}{2D} \tag{5}$$

whereDa is the Darcy number that is obtained by applying the Blasius relation if $2000 < Re < 10^5$:

$$Da = 0.316\cdot Re^{-0.25} \tag{6}$$

2.5. Asymmetrical flow field-flow fractionation (A4F)

The radius of gyration (Rg), hydrodynamic radius (Rh), apparent density (d_{app}), fractal dimension (Df) and shape factor (Rgi(z)/Rhi(z)) of aggregates were determined with an Asymmetrical Flow Field-Flow Fractionation coupled with a Multi-Angle Laser Light Scattering and Differential Refractometer and a Quasi-Elastic Light Scattering (As-FlFFF-MALS-DRi-Qels) system. In an As-FlFFF system macromolecules are separated as a function of their diffusion coefficient, i.e., their hydrodynamic diameter (Dh) during elution.

The As-FlFFF instrument was a DualTec separation system (Wyatt Technology Europe, Dernbach, Germany) with a trapezoidal geometry channel (length: 19.5 cm,; initial width: 1.65 cm; final width: 0.27 cm), with a Mylar spacer of 350 µm and aregenerated cellulose membrane of10 kDa MWCO (Wyatt Technology, Europe) regulated at 22 °C). The mobile phase was aqueous with 45 mM NaCl and 0.02% NaN_3, filtered. With a 100-nm pore size polyvinylidene fluoride membrane (Millipore Corp, Darmstadt, Germany).

The flow method used is described in Table 2. 60 µL of sample with a concentration of 1 $g.L^{-1}$ was injected at a flow of 0.2 mL min^{-1} into the channel.

The As-FlFFF was connected to a Dawn Heleos II multiangle light scattering (MALS) detector (Wyatt Technology, Santa Barbara, CA, USA) operating at a wavelength of 662 nm, and an OptilabRex differential refractive index (dRI) detector (Wyatt Technology, Santa Barbara, CA, USA) operating at a wavelength of 658 nm. A DynaPro NanoStar (Wyatt Technology Europe, Dernbach, Germany) was connected online to the Dawn Heleos II at a 15° angle. Calibration of the MALS unit was performed using toluene. Normalization of the MALS unit and interdetector delays and band broadening calculations were performed with BSA protein.

Processing of light scattering data was done with Astra software, version 7.1.2 (Wyatt Technology). The molar mass and the Rg were obtained with the Berry extrapolation (Berry, 1966) (second-order polynomial fit; refractive index increment: 0.185 ml g^{-1}) This method is adapted for large-size polymers (Aberle et al., 1994) Only seven angles were used for extrapolation, between 57° and 117°. The error percentage is calculated from the difference between the theoretical fit of the Berry model and experimental values.

The apparent densities of each particle, i, $di\,(app)$, were obtained from the molar mass Mwi and Rgi distributions and was calculated as (Glantz et al., 2010; Loiseleux et al., 2018):

$$di\,(app) = \frac{Mwi}{\frac{4}{3}\pi\cdot Rgi\cdot Na} \tag{7}$$

where Na is the Avogadro number.

Shape information was determined from the value of the shape

Table 2
Method used for the characterization of fractal aggregates by A4F, with Vx, the cross flow and Vd, the eluent, laminar parabolic flow.

Time (min)	Mode	Vx start ml/min	Vx end ml/min	Vx/Vd
1	elution	0	0	0
2	focus	2	2	4
6	focus + injection	2	2	4
5	elution	2	2	4
10	elution	2	0.3	4
10	elution	0.3	0.12	0.6
58	elution	0.12	0.12	0.24
15	elution	0	0	0
2	elution + rinsing	0	0	0
6	elution	0	0	0

factor Rgi(z)/Rhi(z), i.e., the ratio between the gyration radius Rgi and the hydrodynamic radius Rhi for the class of particule i weighted by the mass of particles squared (Adolphi and Kulicke, 1997; Brewer and Striegel, 2011, 2010; Burchard, 1983). Theorical values of shape factor may vary from 0.778 for ideal homogeneous spheres, up to 2.36 for a stiff rod (Adolphi and Kulicke, 1997). This ratio provides information about branched or linear structures (Ioan et al., 1999).

The conformation of an object can also be defined by its fractal dimension (Ioan et al., 1999; Loiseleux et al., 2018). The fractal dimension Df for the class of particle i was obtained by the slope of the log-log plot of *Rg* as a function of:

$$Rgi = \frac{1}{Dfi} \cdot Mw \tag{8}$$

2.6. Statistical analysis

The influence of Re, RTh or the temperature (T) have been statistically tested on different variables, namely, the mass fractions of the first, second, third or fourth peak (respectively Mf1, Mf2, Mf3 and Mf4), the gyration radius of the third or fourth peak (respectively Rg3 and Rg 4) and the hydrodynamic radius of the third peak (Rh3). Re, RT_h and T were considered as categorical variables. Analysis of variance (ANOVA) was used to find significant effect of Re, RT_h or T on the different variables, using the Rcmdr package of R software version 3.5.3 (R development Core Team, 2010).

The first model examined the influence of two different categorical variables Re and RT_h on one continuous dependent variable Y. The data are hierarchically structured with RT_h as a nested factor so it is possible to describe the ANOVA model as follows:

$$Y_{ijk} = \mu + \alpha_i + b_{ji} + \varepsilon_{ijk} \tag{9}$$

With μ, the overall mean response, α_i , the effect due to the i-th level of factor Re, b_{ji},the effect due to the j-th level of factor RT_h nested within Re and ε_{ijk} called residual error.

The second model examined the influence of T on one continuous dependent variable Y. The model for this one-way ANOVA can be commonly described by:

$$Y_{ijk} = \mu + \alpha_i \varepsilon_{ijk} \tag{10}$$

With μ, the overall mean response, α_i , the effect due to the i-th level of factor Temperature and ε_{ijk} called residual error.

Only effects significant at the $p < 0.05$ level have been considered and will be discussed.

2.7. Determination of the level of βlg denaturation and kinetic parameters

The evolution of the βlg denaturation level with time and temperature was performed using a HPLC chromatographic system (Waters, Milford, MA, USA). The method used is described in a previous study (Petit et al., 2011). Lyophilized βlg powder (purity ≥ 90%) was used as the standard and obtained from Sigma-Aldrich (St. Louis, MO, USA).

3. Results and discussion

3.1. Characterization of aggregates formed under continuous processing conditions

As mentioned above, each processing condition was tested in duplicate, showing satisfactory repeatability. Fig. 3 shows the representative concentration profile and gyration radius obtained for fractal aggregates formed at 80 °C under different conditions of Reynolds number and RT_h, using As-FlFFF-MALS-DRi-Qels. The factogram makes it possible to distinguish three distinct populations of protein and aggregates. Table 3 represents the characteristics of each eluted population.

The first population, eluted between 10 and 18 min, represents non-aggregated WPs and caseins present in the powder. Indeed, according to the literature, βlg denatures and aggregates after heat treatment, but other WPs do not necessarily do so. Table 3 shows that the rate of non-aggregated species represented by the first peak varied slightly depending on the conditions and was in the range of 23 w/w%. This value was consistent with the sum of the non-denatured-aggregated whey proteins revealed by quantitative analysis after precipitation at pH 4.6 (approx. 11 w/w% of the protein) and the casein present that were eluted in the first peak as well (7.3 w/w%).

The second population eluted between 18 and 33 min was attributed to primary aggregates, with an Rg of 60 nm.

Finally, the third population eluted between 33 and 60 min was assimilated to fractal aggregates with a mean Rg of 152–222 nm, depending on process conditions (Table 3). Information about shape and molecular architecture of these aggregates given by their shape factor (Rg/Rh) was consistent with this assumption. The average shape factor of the third eluted peak was comparable for the three samples - in between 1.0 and 1.2 - which implies a rather elongated fractal structure. Moreover, their fractal dimension (Df) ranged from 2.1 to 2.4 for the three process conditions. This was consistent with a branched morphology in agreement with the results published by Loiseleux et al. (2018) and Mahmoudi et al. (2014) who reported a Df value of 2.1 and a range of 2.15–2.19 for fractal aggregates, respectively. It was not possible to evaluate the shape factor or fractal dimension of the first and second eluted peak because of the method that only apples to large objects.

3.2. Influence of flow regime and heating residence time

In order to distinguish clearly the influence of the flow regime on the formation of aggregates, the Moody diagram of the indirect Joule effect Actijoule heat exchanger was established. Fig. 4 indicates that the flow regime was laminar below Re 2500, transient at intermediate Re values ranging from 2500 to 5000 and, finally, turbulent above Re 5000. Experiments conducted at Re 2000 (condition 2; Table 1), Re 3200 (condition 5; Table 1) and Re 6900 (conditions 1,3,4; Table 1) therefore made it possible to scan the effect of the different flow regimes.

As mentioned above, non-aggregated protein present in the first peak represented a mass fraction of approximately 23 w/w%. This means that the extent of denaturation aggregation was in the same range, regardless of the processing conditions, and that the same proportion of WP aggregated to form primary or secondary aggregates. Indeed, there is no significant effect of Re or RTh on the mass fraction of the first peak (p-value: 0.58 and 0.22 respectively). However, the distribution between primary and secondary quantitatively varied depending on the process conditions. Indeed, the lower the Re value and the longer the RT_h were, the higher the mass fraction of the third eluted population corresponding to secondary aggregates (Table 3).

On the other hand, fractal aggregates qualitatively varied according to the process conditions. Indeed, aggregates were denser under transient or turbulent conditions. This was in agreement with the work of Kolb and Jullien (1984) who suggested that aggregates formed by chemical aggregation were denser than those formed by diffusive aggregation since the encounter probability between two entities increased with turbulence. Moreover, larger aggregates were produced at intermediate Reynolds numbers and RT_h (Rg = 222 nm for Re 3200, with RT_h = 15 s) compared to those produced at extreme values of Re and of RT_h (Rg ≤ 183.2 nm for Re 2000 with RT_h = 230 s, or Re 6900 with RT_h = 7 s; Table 3). The shape factor and the value of the fractal dimension of aggregates obtained for the intermediate flow regime are consistent with a more open structure. These findings are in agreement with previous studies (Simmons et al., 2007; Wolz et al., 2016). Indeed, Simmons et al. (2007) and Wolz et al. (2016) reported that the

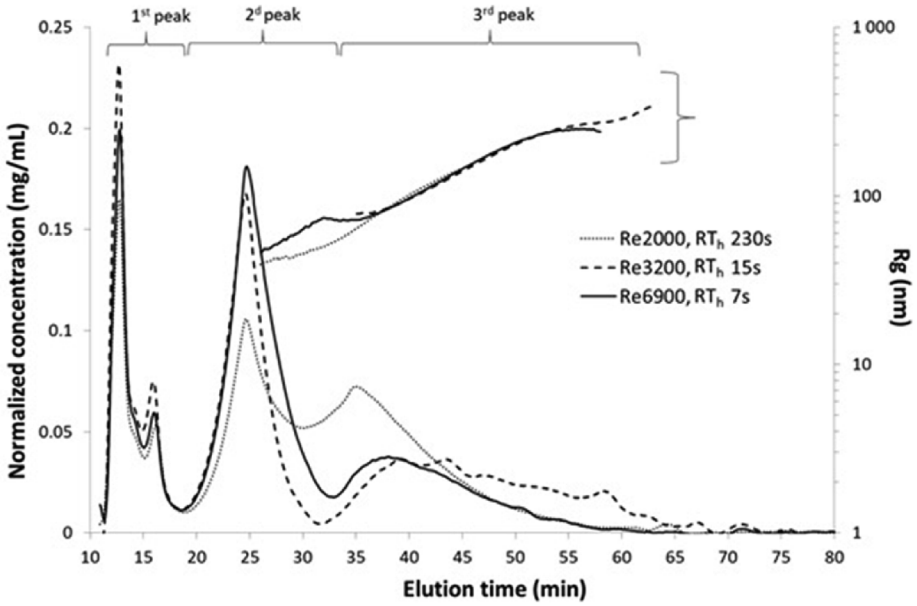

Fig. 3. Typical A4F fractograms representing normalized concentrations (left axis) and gyration radius distributions (right axis) of fractal aggregates produced under different flow regime conditions, characterized by the Reynolds number (Re) and heating residence time (RT_h). Experiments were done in duplicate and gave the same trend and mean values.

aggregate size reached a maximum at the intermediate shear rate using a Couette system. On the other hand, Kerche et al. (2016) did not observe any dependence between aggregate size and shear or flow regime within a tubular exchanger. Erabit et al. (2014) observed no effect of shear rate on denaturation rate and concluded that shear would not affect the collision of monomers.

As shown in Eq. (1), the Re number is a function of the flow velocity that simultaneously affected RT_h. In order to determine the respective influence of heating residence time and flow regime on the size of fractal aggregates, experiments were conducted using different inner tube diameter/flow rate ratios to obtain a constant Reynolds value with short (7 s), medium (46 s) or long (69 s) RT_h values (conditions 1.3 and 4; Table 1). The results are presented in Fig. 5 and Table 4.

Fig. 5 shows that the same three peaks and corresponding aggregate populations were obtained as previously observed (Fig. 3) and regardless of the RT_h conditions. Moreover, no shift of the third peak toward the formation of larger aggregates could be obtained by varying the RT_h value, and Rg values remained in the same range regardless of the latter ($Rg \leq 196.3$ nm; Table 4).

Similarly, Df and shape factor values did not significantly evolve and remained in agreement with a fractal structure. Similar experiments with varying RT_h at a constant Reynolds number of 2000 led to the same conclusion, i.e., no differences in the characteristics of the formed aggregates (data not shown).

In order to obtain quantitative estimations of the effects of Re and RT_h, analysis of variance (ANOVA) was performed. The variation of the distribution between primary and secondary aggregates was due to Re only, indeed Re had a significant effect on Mf2 (p-value: 0.04), and Mf3 (p-value: 0.03) whereas RT_h had no significant effect on Mf2 (p-value: 0.21) and Mf3 (p-value: 0.09). Moreover, the increase of aggregate size producted at intermediate Re and RT_h is only due to the effect of Re. Indeed, Re had a significant effect on Rg3 (p-value: 0.01) and Rh3 (p-value: 0.003) whereas RT_h had no significant effect on Rg3 (p-value: 0.09) and Rh3 (p-value: 0.08). It can therefore be concluded that the flow regime influenced the aggregate size in the range of tested conditions since a significant increase of aggregate size could be obtained under intermediate flow regime conditions. Conversely, aggregate size was not affected by RT_h.

3.3. Impact of heating temperature

Fig. 6 shows the concentration profile and the gyration radius obtained for fractal aggregates formed at heating temperatures ranging from 70 °C to 90 °C under constant flow regime and heating residence time conditions (Re = 6900, RT_h = 7 s; condition 4, Table 1). Table 5 gives the characteristics of each population eluted.

At 70 °C, the factogram reveals the presence of only two peaks corresponding to non-aggregated whey proteins for the first one, and to primary aggregates for the second one, which is demonstrated by the fact that secondary fractal aggregates were not formed at this temperature.

Beyond 85 °C, a new fourth population of large aggregates ($Rg \geq 289.7$ nm; Table 5) appears at elution time between 50 and 80 min. At 85 °C, these aggregates present a shape factor close to that of the aggregates of the third peak, compatible with a fractal structure. It is important to note that the fractionation method did not make it possible to separate the aggregates formed at 90 °C. Indeed the membrane was clogged, the recovery rate was weak, and the Rh signal presented many interferences, making it impossible to estimate the shape factor at this temperature. This formation of larger aggregates at

Table 3
Comparison of Kolmogorov scale (l_k), rate of native protein, mass fraction, shape factor (Rg/Rh), fractal dimension (Df), gyration radius (Rg) and apparent density (d(app)) of different populations of aggregates, corresponding to different peaks eluted by A4F under different process conditions.

Sample		l_k (μm)	Native protein (w/w %) after precipitation at pH 4.6	1st peak	2nd peak	3rd peak				
Re	RT_h (s)			Mass fraction (w/w %)	Mass fraction (w/w %)	Mass fraction (w/w %)	Rg/Rh	Df	Rg (nm)	d(app) (10^3 kg m^{-3})
2000	230	–	9.8	20.9	36.7	42.4	1.1	2.4	152.4 (± 1.9%)	0.39
3200	15	–	12.5	25.6	38	36.4	1.2	2.1	222.0 (± 1.10%)	1.14
6900	7	21.8	11.1	22.6	51.1	26.3	1.0	2.3	183.2 (± 1.2%)	0.98

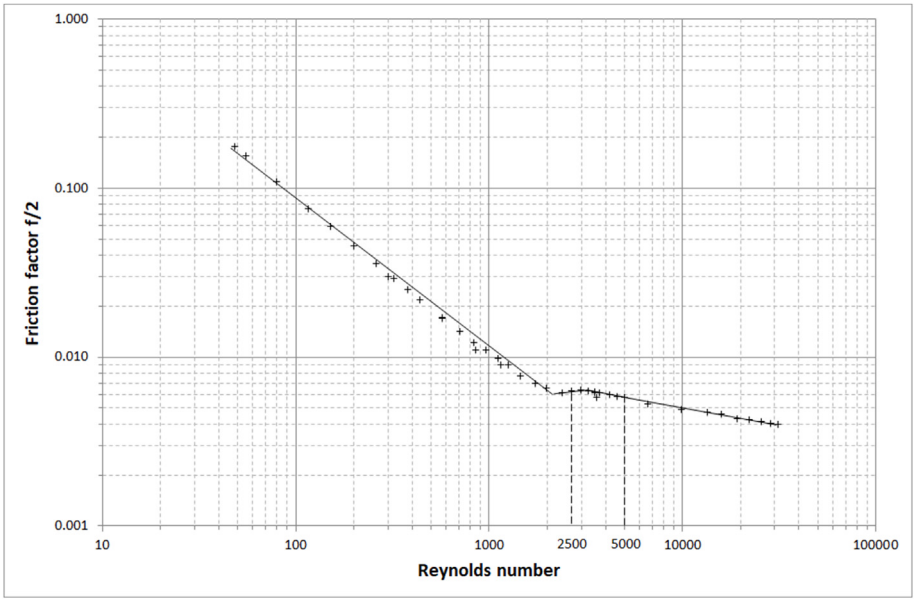

Fig. 4. Moody diagram characterizing flow regime in the tubular heat exchanger Actini.

a temperature above 80 °C is in agreement with the results of Mahmoudi et al. (2014) who showed an increase of aggregate Rg from 35 nm at 70 °C to 100 nm at 100 °C, while the aggregate shape simultaneously evolved towards a spherical morphology. These Rg values were smaller than those obtained in this study because of different initial protein solution conditions (15 $g.L^{-1}$ protein and 3 mM NaCl).

The same influence of heating temperature was observed under a transient flow regime (Re = 3200, RT_h = 15 s) (data not shown). Moreover, a statistical validation have been conducted that reveal a significant effect of T on Mf3, Rg3, Mf4 and Rg4 with p-values of 0.0009; 0.0005; 0.0002 and 0.0003 respectively, confirming that temperature is a key lever to drive aggregate characteristics beyond the influence of the flow regime previously revealed in this study. This conclusion is in agreement with the study of Simmons et al. (2007) who showed that the dependence of aggregate size on shear rate decreased with increasing temperature.

3.3.1. Mechanisms involved in the formation of fractal aggregates by continuous processing

Simmons et al. (2007) suggested that the final size of aggregates depended on particle collision or breakage, i.e., aggregates were built either by assembly or by fragmentation. However, breakage would induce aggregates with a spherical aspect and non-fractal shape (Mahmoudi et al., 2014), which were not observed in this study. Moreover, the size of the flow eddies was evaluated through the Kolmogorov length in turbulent regime (Tables 3 and 4). The values obtained were 100–400 times greater than the maximum aggregate Rg values. As evidence of this, the more turbulent flow conditions were unable to induce fragmentation of the aggregates in the course of their formation. It is thus possible to assume that fractal aggregates, within the continuous processing conditions implemented in this study, should form and grow through an association mechanism rather than a breakage mechanism.

As previously mentioned, the aggregation step involves the association of reactive material, i.e., unfolded/denatured protein. Fig. 7,

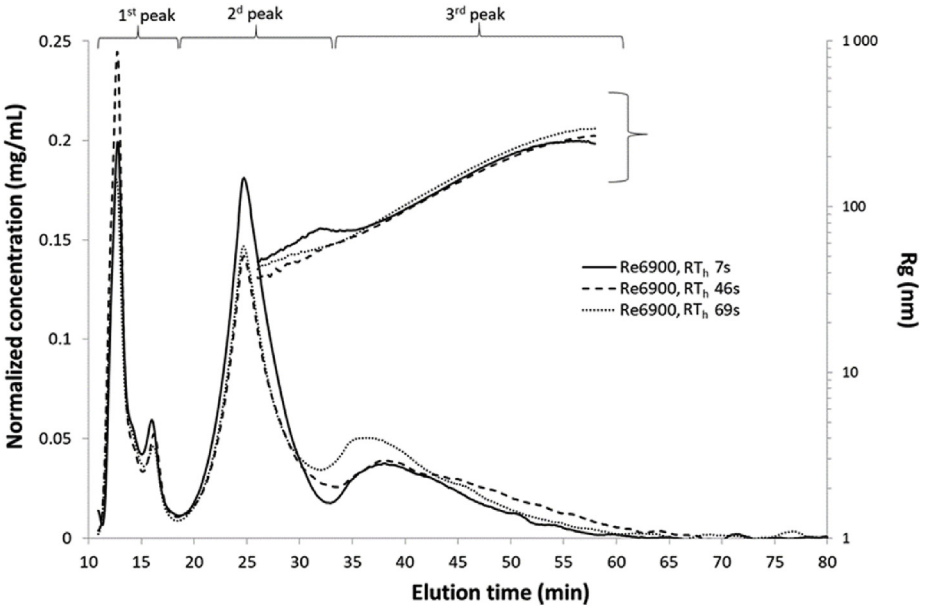

Fig. 5. Typical A4F fractograms representing normalized concentration (left axis) and gyration radius distribution (right axis) of fractal aggregates produced under different heating residence time RT_h for constant flow regime conditions (Re = 6900). Experiments were realized in duplicate and gave the same trend and mean values.

Table 4
Comparison of Kolmogorov scale (l_k), mass fraction, shape factor (Rg/Rh), fractal dimension (Df) and gyration radius (Rg) of different population of aggregates, corresponding to different peaks eluted by A4F. Aggregates were produced under the same flow regime conditions (Re = 6900) and different conditions of heating residence time (RT_h).

Sample		l_k(µm)	1st peak	2nd peak	3rd peak			
Re	RT_h (s)		Mass fraction (w/w %)	Mass fraction (w/w %)	Mass fraction (w/w %)	Df	Rg/Rh	Rg (nm)
6900	7	21.84	2.6	51.1	26.3	2.3	1.0	183.2 (± 1.2%)
6900	46	65.72	31.3	49.3	19.4	2.2	1.3	196.3 (± 1.4%)
6900	69	82.18	21.5	41.1	37.4	2.1	1.3	193.9 (± 1.5%)

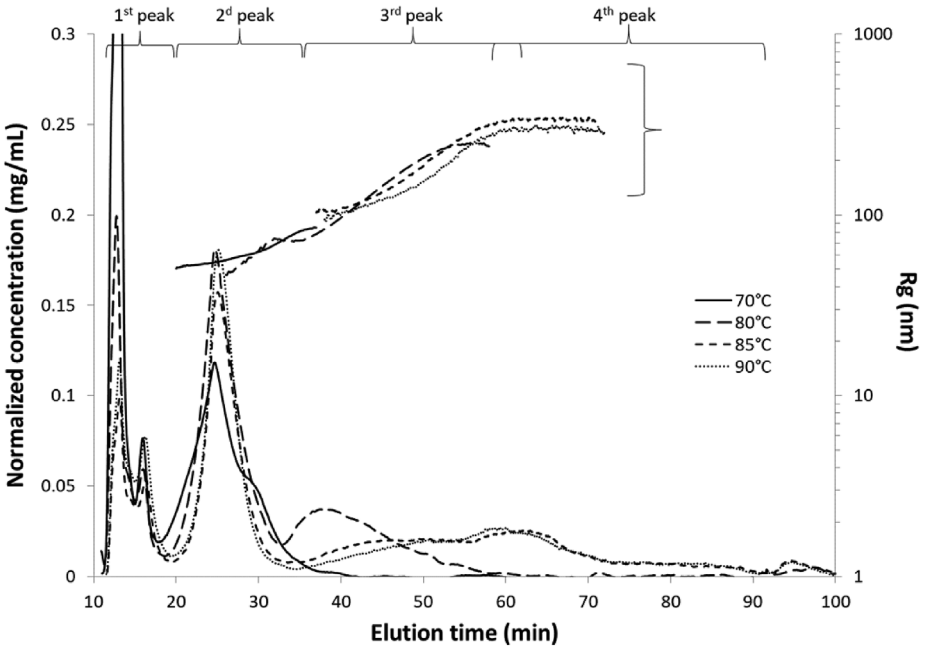

Fig. 6. Typical A4F fractograms representing normalized concentration (left axis) and gyration radius distribution (right axis) of fractal aggregates produced at heating temperature ranging from 70 °C to 90 °C with constant flow regime and heating residence time conditions (Re = 6900, RT_h = 7s). Experiments were realized in duplicate and gave the same trend and mean values.

Table 5
Comparison of mass fraction, shape factor (Rg/Rh), fractal dimension (Df) and gyration radius (Rg) for different populations of aggregates, corresponding to different peaks eluted by A4F. Aggregates were produced under the same flow regime and RT_h (Re 6900, RT_h 7s) conditions, but at different heating temperatures ranging from 70 °C to 90 °C.

Sample	1st peak	2nd peak	3rd peak				4th peak			
Heating temperature (°C)	Mass fraction (w/w %)	Mass fraction (w/w %)	Mass fraction (w/w %)	Df	Rg/Rh moy	Rg (nm)	Mass fraction (w/w %)	Df	Rg/Rh	Rg (nm)
70	54.4	45.6	0	–	–	–	0	–	–	–
80	22.6	51.1	26.3	2.3	1.0	183.2 (± 1.2%)	0	–	–	–
85	16.8	40.4	20.2	2.6	1.3	219.4 (± 4.1%)	22.6	–	1.4	331.1 (± 3.8%)
90	21	41.2	14.6	–	–	171.5 (± 5.7%)	23.2	–	–	289.7 (± 5.1%)

representing the Arrhenius plot of Blg denaturation in the WPI tested in this study, provided information about unfolding and aggregation kinetics as a function of heating temperature. The transition between the unfolding and aggregation curves occurred at a temperature of 78 °C, in accordance with the results published by Petit et al. (2011). Using this Arrhenius representation, it was possible to estimate the level of denaturation of βlg (that is to say the mass fraction of unfolded βlg) within the processing time-temperature conditions and for the different RT_h tested (Fig. 8). It is shown that regardless of RT_h, 100% of βlg was unfolded at the exit of the heating zone and no additional reactive material should be expected while increasing heating residence time. As the amount of reactive material was limited, it explains why RT_h was shown to have no influence on the final size of the aggregates. Conversely, the larger aggregates formed above 80 °C would result from the instantaneous unfolding of βlg within this range of temperature, enhancing the encounter of reactive species.

Regarding the influence of flow conditions, it was shown that the aggregate size was positively and significantly influenced under intermediate flow regime. Given the fact that to date and to the best of author knowledge, no studies dealt with the impact of flow regime on denaturation-aggregation of protein, an analogy was sought with well studied processes involving two nucleation-growth steps such as crystallisation. Indeed, recent studies (Forsyth et al. (2015) and Nappo et al. (2018)) showed a strong increase of nucleation rate with shear rate, namely in the frame of their study with increasing Re value. This support the idea that the nucleation rate of protein aggregates would be minimal in laminar regime compared to turbulent conditions, leading to a more limited number of available nucleation points at low Re values. As underlined above, βlg unfolding is complete regardless of the process conditions. However, limiting the nucleation points would lead

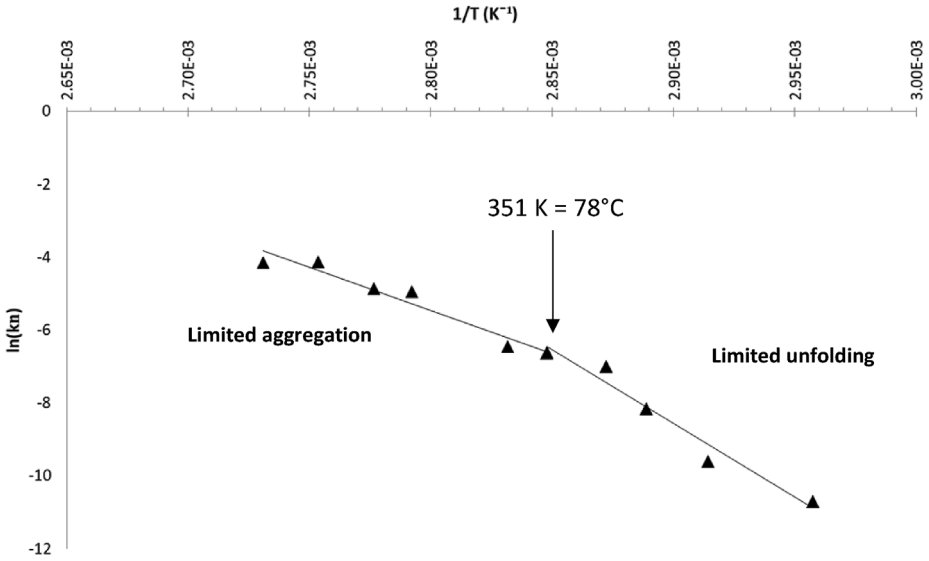

Fig. 7. Arrhenius plot of β-lactoglobulin denaturation in the whey protein isolate used in this study. Plot lines are a guide for the eyes.

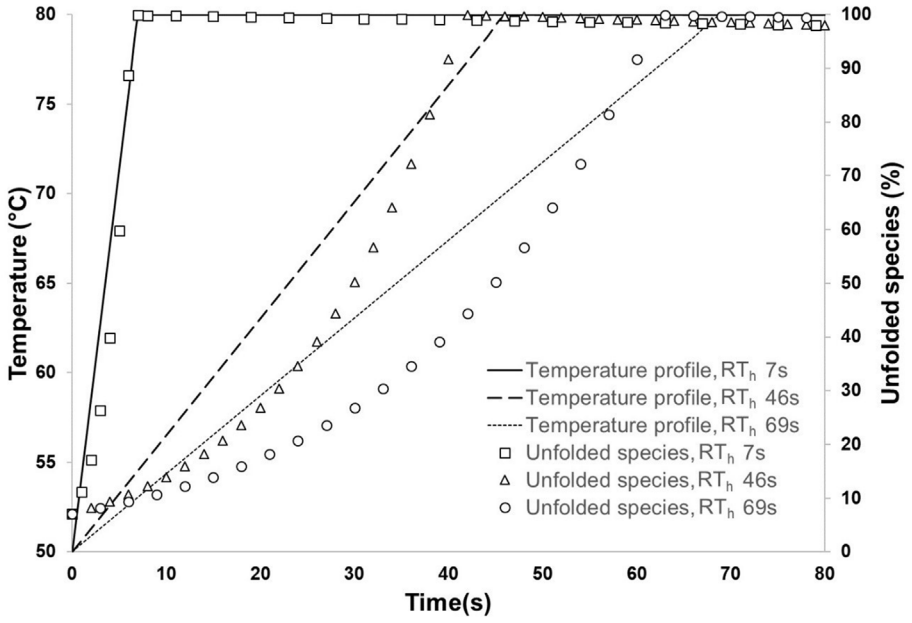

Fig. 8. Impact of heating residence time (RT_h) on the generation of unfolded species at 80 °C. Temperature profile: Bold line/Re = 6900, RT_h = 7 s; dotted line/Re = 6900, RT_h = 46 s; point line/Re = 6900, RT_h = 69 s. Unfolded species (%): white square/Re = 6900, RT_h = 7 s; white triangle/Re = 6900, RT_h = 46 s; white circle/Re = 6900, RT_h = 69 s.

to preferential secondary aggregate formation (higher mass fraction collected in 3rd peak, Table 3). Moreover and as the flow is distributed into distinct streamlines in laminar conditions, the reactive protein species able to aggregate together is expected to be limited to the one present in each streamline. This local depletion of the reactive protein species would explain the smaller Rg value of the third peak, despite the limited number of nucleation points.

Conversely, the high nucleation rate expected in a turbulent flow regime would first favor the creation of numerous nucleation points and then the growth of aggregates. This would lead to a consumption of denatured protein into a large number of primary aggregates, and to the consumption of the available reactive species before obtaining large-size secondary aggregates. In fact, the mass fraction of primary aggregates represented 51% instead of less than 40% in the laminar regime (Table 3).

The transient flow regime was shown to maximize aggregate size: the aggregate nucleation would be here favored compared to a laminar regime, but not as much as for a turbulent flow regime. Consequently, the reactive species would be directed towards a smaller number of nucleation points than in a turbulent regime, favoring the growth of secondary aggregates. Indeed, the Rg of the third peak was approximately 220 nm, i.e., larger than the aggregates obtained under laminar or turbulent flow regime conditions (Table 3).

To sum up and for better understanding, Fig. 9 provides a schematic representation of the possible mechanisms involved in the formation of aggregates depending on the flow regime conditions.

4. Conclusions

To conclude, the scale-up of the continuous production process of fractal aggregates was conducted in a pilot line composed of indirect Joule effect heat exchangers. Process parameters were studied as levers to modulate the size and shape of WP aggregates. Flow regime and heating temperature as well were shown to have a significant impact on aggregate size. Indeed, a transient regime led to larger aggregates compared to laminar and turbulent flow, which would be due to the encounter between optimal reactive species. Even larger fractal aggregates were obtained when increasing the heating temperature

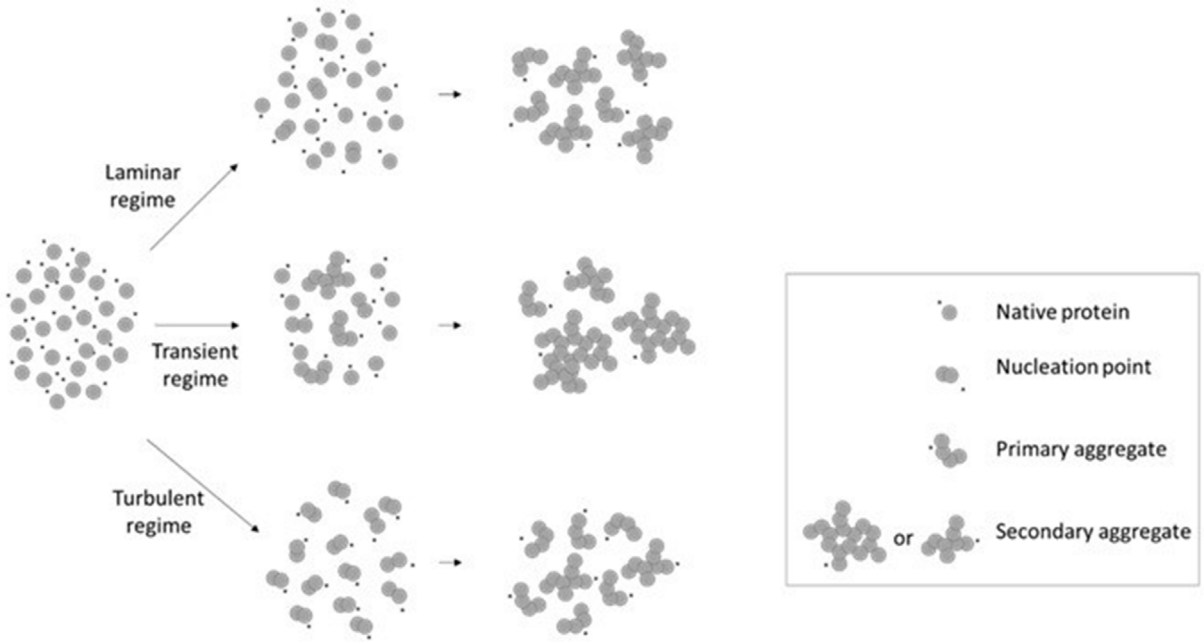

Fig. 9. Schematic representation of the formation of WP aggregates depending on different flow regime conditions.

beyond 85 °C since the unfolding-aggregation of WP was controlled by the aggregation step under such conditions. Moreover, residence time in the heating section showed no effect on the size and shape of the aggregates formed. This study is a first approach to control aggregate properties obtained in a continuous dynamic mode.

Conflicts of interest

On behalf of the authors and as corresponding author, I confirm that there are no known conflicts of interest associated with this publication and there has been no financial support for this work that could have influenced its outcome.

Declarations of interest

None.

Acknowledgements

We would like to thank the BBA industrial association and the Regional Councils of Brittany (grant n° 13008651) and Pays de la Loire (grant n° 2014-07081) who funded this work through the interregional PROFIL project, carried out by the association “Pole Agronomique Ouest”. We also thank Dr. J. Leonil of INRA for the scientific co-ordination.

Appendix A. Supplementary data

Supplementary data to this article can be found online at https://doi.org/10.1016/j.jfoodeng.2019.07.022.

References

Aberle, T., Burchard, W., Vorwerg, W., Radosta, S., 1994. Conformational contributions of amylose and amylopectin to the structural properties of starches from various sources. Starch - Stärke 46, 329–335. https://doi.org/10.1002/star.19940460903.

Adolphi, U., Kulicke, W.-M., 1997. Coil dimensions and conformation of macromolecules in aqueous media from flow field-flow fractionation/multi-angle laser light scattering illustrated by studies on pullulan. Polymer 38, 1513–1519. https://doi.org/10.1016/S0032-3861(96)00675-1.

Berry, G.C., 1966. Thermodynamic and conformational properties of polystyrene. I. Light-Scattering studies on dilute solutions of linear polystyrenes. J. Chem. Phys. 44, 4550–4564. https://doi.org/10.1063/1.1726673.

Bon, C.L., Nicolai, T., Durand, D., 1999. Growth and structure of aggregates of heat-denatured β-Lactoglobulin. Int. J. Food Sci. Technol. 34, 451–465. https://doi.org/10.1046/j.1365-2621.1999.00310.x.

Brewer, A.K., Striegel, A.M., 2011. Characterizing the size, shape, and compactness of a polydisperse prolate ellipsoidal particle via quadruple-detector hydrodynamic chromatography. Analyst 136, 515–519. https://doi.org/10.1039/C0AN00738B.

Brewer, A.K., Striegel, A.M., 2010. Hydrodynamic Chromatography of Latex Blends - Brewer - 2010 - Journal of Separation Science. Wiley Online Library [WWW Document]. URL. https://onlinelibrary.wiley.com/doi/full/10.1002/jssc.201000565 accessed 2.22.19.

Buggy, A.K., McManus, J.J., Brodkorb, A., Hogan, S.A., Fenelon, M.A., 2018. Pilot-scale formation of whey protein aggregates determine the stability of heat-treated whey protein solutions—effect of pH and protein concentration. J. Dairy Sci. 101, 10819–10830. https://doi.org/10.3168/jds.2017-14177.

Burchard, W., 1983. Static and dynamic light scattering from branched polymers and biopolymers. In: Light Scattering from Polymers, Advances in Polymer Science. Springer Berlin Heidelberg, pp. 1–124.

Chevallier, M., Riaublanc, A., Lopez, C., Hamon, P., Rousseau, F., Thevenot, J., Croguennec, T., 2016. Increasing the heat stability of whey protein-rich emulsions by combining the functional role of WPM and caseins. Food Hydrocolloids. https://doi.org/10.1016/j.foodhyd.2016.12.014.

Erabit, N., Flick, D., Alvarez, G., 2014. Formation of β-lactoglobulin aggregates during thermomechanical treatments under controlled shear and temperature conditions. J. Food Eng. 120, 57–68. https://doi.org/10.1016/j.jfoodeng.2013.07.003.

Erabit, N., Ndoye, F.T., Alvarez, G., Flick, D., 2016. Coupling population balance model and residence time distribution for pilot-scale modelling of β-lactoglobulin aggregation process. J. Food Eng. 177, 31–41. https://doi.org/10.1016/j.jfoodeng.2015.12.013.

Forsyth, Carol, Mulheran, P.A., Forsyth, Claire, Haw, M.D., Burns, I.S., Sefcik, J., 2015. Influence of controlled fluid shear on nucleation rates in Glycine aqueous solutions. Cryst. Growth Des. 15, 94–102. https://doi.org/10.1021/cg5008878.

Glantz, M., Håkansson, A., Lindmark Månsson, H., Paulsson, M., Nilsson, L., 2010. Revealing the size, conformation, and shape of casein micelles and aggregates with asymmetrical flow field-flow fractionation and multiangle light scattering. Langmuir 26, 12585–12591. https://doi.org/10.1021/la101892x.

Inthavong, W., Kharlamova, A., Chassenieux, C., Nicolai, T., 2016. Structure and flow of dense suspensions of protein fractal aggregates in comparison with microgels. Soft Matter 12, 2785–2793. https://doi.org/10.1039/c5sm02893k.

Ioan, C.E., Aberle, T., Burchard, W., 1999. Solution properties of glycogen. 1. Dilute solutions. Macromolecules 32, 7444–7453. https://doi.org/10.1021/ma990600m.

Jung, J.-M., Savin, G., Pouzot, M., Schmitt, C., Mezzenga, R., 2008. Structure of heat-induced β-lactoglobulin aggregates and their complexes with sodium-dodecyl sulfate. Biomacromolecules 9, 2477–2486. https://doi.org/10.1021/bm800502j.

Kang, D.Y., Moon, J.M., Lee, S., 2011. Comparison of size-exclusion chromatography and flow field-flow fractionation for separation of whey proteins. Bull. Korean Chem. Soc. 32, 1315–1320. https://doi.org/10.5012/bkcs.2011.32.4.1315.

Kerche, F., Weterings, M., Beyrer, M., 2016. The effect of temperature and shear upon technological properties of whey protein concentrate: aggregation in a tubular heat exchanger. Int. Dairy J. 60, 32–38. https://doi.org/10.1016/j.idairyj.2016.02.032.

Kharlamova, A., Chassenieux, C., Nicolai, T., 2018a. Acid-induced gelation of whey protein aggregates: kinetics, gel structure and rheological properties. Food

Hydrocolloids 81, 263–272. https://doi.org/10.1016/j.foodhyd.2018.02.043.
Kharlamova, A., Nicolai, T., Chassenieux, C., 2018b. Calcium-induced gelation of whey protein aggregates: kinetics, structure and rheological properties. Food Hydrocolloids 79, 145–157. https://doi.org/10.1016/j.foodhyd.2017.11.049.
Kolb, M., Jullien, R., 1984. Chemically limited versus diffusion limited aggregation. J. Phyique Lett. 45, 977–981. https://doi.org/10.1051/jphyslet:019840045020097700.
Loiseleux, T., 2018. Compétition interfaciale entre protéines solubles et agrégées : connectivité des goutelettes et texture des émulsions laitières.
Loiseleux, T., Rolland-Sabaté, A., Garnier, C., Croguennec, T., Guilois, S., Anton, M., Riaublanc, A., 2018. Determination of hydro-colloidal characteristics of milk protein aggregates using asymmetrical flow field-flow fractionation coupled with multiangle laser light scattering and differential refractometer (AF4-MALLS-DRi). Food Hydrocolloids. https://doi.org/10.1016/j.foodhyd.2017.08.012.
Mahmoudi, N., Gaillard, C., Riaublanc, A., Boue, F., Axelos, M.A.V., 2014. Transition from fractal to spherical aggregates of globular proteins: Brownian-like activation and/or hydrodynamic stress? Curr. Top. Med. Chem. 14, 630–639.
Mahmoudi, N., Mehalebi, S., Nicolai, T., Durand, D., Riaublanc, A., 2007. Light-scattering study of the structure of aggregates and gels formed by heat-denatured whey protein isolate and β-lactoglobulin at neutral pH. J. Agric. Food Chem. 55, 3104–3111. https://doi.org/10.1021/jf063029g.
Nappo, V., Sullivan, R., Davey, R., Kuhn, S., Gavriilidis, A., Mazzei, L., 2018. Effect of shear rate on primary nucleation of para-amino benzoic acid in solution under different fluid dynamic conditions. Chem. Eng. Res. Des. 136, 48–56. https://doi.org/10.1016/j.cherd.2018.04.039.
Nicolai, T., Britten, M., Schmitt, C., 2011. β-Lactoglobulin and WPI aggregates: formation, structure and applications. Food Hydrocolloids, 25 years of Advances in. Food Hydrocolloid Research 25, 1945–1962. https://doi.org/10.1016/j.foodhyd.2011.02.006.
Nicorescu, I., Loisel, C., Riaublanc, A., Vial, C., Djelveh, G., Cuvelier, G., Legrand, J., 2009. Effect of dynamic heat treatment on the physical properties of whey protein foams. Food Hydrocolloids 23, 1209–1219. https://doi.org/10.1016/j.foodhyd.2008.09.005.
Petit, J., Herbig, A.-L., Moreau, A., Delaplace, G., 2011. Influence of calcium on β-lactoglobulin denaturation kinetics: implications in unfolding and aggregation mechanisms. J. Dairy Sci. 94, 5794–5810. https://doi.org/10.3168/jds.2011-4470.
Pouzot, M., Nicolai, T., Visschers, R.W., Weijers, M., 2005. X-ray and light scattering study of the structure of large protein aggregates at neutral pH. Food Hydrocolloids 19, 231–238. https://doi.org/10.1016/j.foodhyd.2004.06.003.
Simmons, M.J.H., Jayaraman, P., Fryer, P.J., 2007. The effect of temperature and shear rate upon the aggregation of whey protein and its implications for milk fouling. J. Food Eng. 79, 517–528. https://doi.org/10.1016/j.jfoodeng.2006.02.013.
Wijayanti, H.B., Bansal, N., Deeth, H.C., 2014. Stability of whey proteins during thermal processing: a review. Compr. Rev. Food Sci. Food Saf. 13, 1235–1251. https://doi.org/10.1111/1541-4337.12105.
Wolz, M., Mersch, E., Kulozik, U., 2016. Thermal aggregation of whey proteins under shear stress. Food Hydrocolloids 56, 396–404. https://doi.org/10.1016/j.foodhyd.2015.12.036.